ACS OMEGA

Open Access

This article is licensed under CC-BY-NC-ND 4.0

http://pubs.acs.org/journal/acsodf

Article

Eco-Friendly *Piper cubeba* Official Extract Corrosion Inhibition of C-Steel in 1 M Sulfamic Acid

Aya. M. Salem* and Merfat S. Al-Sharif*

Cite This: *ACS Omega* 2024, 9, 5024−5037

Read Online

ACCESS | Metrics & More | Article Recommendations

ABSTRACT: This work offers a high-performing, environmentally friendly corrosion inhibitor for carbon steel in 1 M sulfamic acid (H_2NSO_3H). Potentiodynamic polarization and electrochemical impedance spectroscopy were used to evaluate the anticorrosion properties of *Pipper cubeba* official extract (P.cubebaOE) for carbon steel in 1 M H_2NSO_3H at 25 to 45 °C. At a temperature of 45 °C, the P.cubebaOE reached a maximum corrosion inhibition efficiency of 96%. P.cubebaOE was also subjected to Fourier transform infrared spectroscopy in order to ascertain its primary chemical composition. Additionally, the behavior of P.cubebaOE in terms of corrosion inhibition on carbon steel was examined at the microscopic level using scanning electron microscopy. The findings demonstrate that P.cubebaOE's adsorption type on carbon steel conforms to the Langmuir adsorption isotherm model. Based on the adsorption isotherm model, the free energy was estimated to be approximately −20.0 kJ/mol, suggesting that P.cubebaOE is physically adsorbing on the surface of carbon steel. The results of the density functional theory and molecular dynamics simulations show that P.cubebaOE exhibits excellent inhibition performance on carbon steel in H_2NSO_3H solution and are consistent with the electrochemical experimental results. This work offers significant information on the development of environmentally friendly corrosion inhibitors for carbon steel.

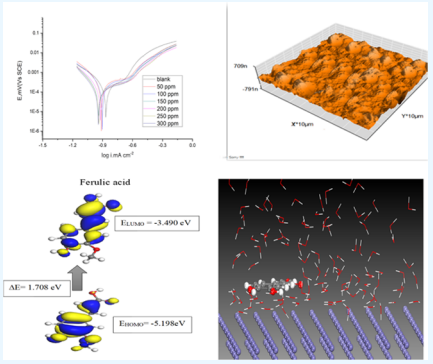

1. INTRODUCTION

Metal corrosion is now a critical concern in a variety of sectors and the environment. As a result, efforts must be undertaken to lower the corrosion risks across many businesses. Inhibitors are added in insignificant amounts to the corrosive media to protect metals against corrosion-induced dissolution, which has a significant practical benefit.[1−5] Due to these compounds' high toxicity, there is a shortage of their inhibitors, which has prompted researchers to look for more environmentally friendly substitutes with functional groups that include sulfur, nitrogen, or oxygen atoms and have been approved as corrosion inhibitors.[6,7] The last 10 years have seen an increase in curiosity about environmentally friendly products as a result of new environmental laws and heightened environmental awareness. Natural substitutes have been employed for their antibacterial, antifungal, anticancer, and antimicrobial properties.[8−13] Many attempts are underway to create substances appropriate for use as anticorrosion agents in entertainment applications. The foundation of this research is the use of plant extracts that are safe for the environment to prevent metal and alloy corrosion. The use of plant extracts as corrosion barriers is supported by the research listed below. The extract of calicotome,[14] Hibiscus rosa-sinensis Linn[15] Spirulina solution verified by electrochemical methods,[17] beet root extract in well water,[16] spirulina.[18] Finding a naturally occurring, inexpensive, and ecologically friendly chemical that might be utilized to prevent corrosion of C-steel is the goal of the current research. Utilizing natural resources will enable the achievement of both economic and environmental objectives. In several researches, plant extracts have been mentioned as prospective agents to lessen corrosion in different industrial solutions.[19−31] As reported previously, the ethanolic extract of (P.cubebaOE) contains levels of Yatein, Cbenin, cubebinone, cubebininolide, Hinokinin and cubebinin, single aldehyde, and α, β-unsaturated ketone. From the *Piper cubeba*, several phenolic acids and flavonoids have been found and extracted. In addition to rutin (8 ppm) and catechin (5 ppm), researchers found that the aqueous extract of *P. cubeba* fruits also contained Gallic acid (8 ppm), caffeic acid (13 ppm), syringic acid (3 ppm), and ferulic acid (11 ppm).[32] The aqueous extract from the same study contained 2.11 mg/g of total phenols.[33] According to certain literature, each of the four ingredients' centers of adsorption are oxygen atoms and aromatic rings.[33,34] Consequently, P.cubebaOE could be investigated as a corrosion inhibitor that is friendly to the environment. Our work examined the inhibitory effect of this extract on C-steel in 1.0 M H_2NSO_3H acid using a classical

Received: November 24, 2023
Revised: December 26, 2023
Accepted: January 3, 2024
Published: January 12, 2024

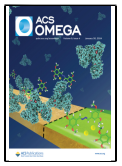

© 2024 The Authors. Published by American Chemical Society

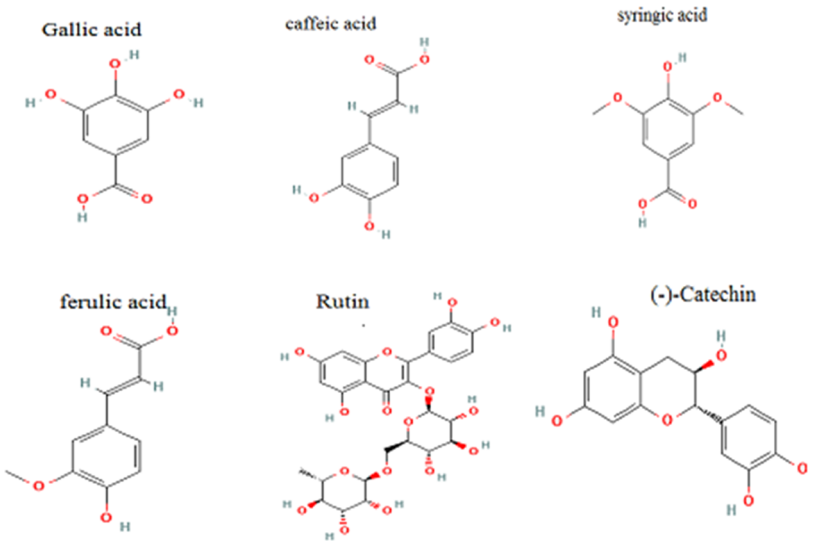

Figure 1. P.CubebaOE primary ingredient chemical composition.

Table 1. Lists the Chemical Details of the Contents of the Pieces of C-Steel

element	Fe	C	Mn	P	Si	Cr	Co
weight %	balance	0.200	0.600	0.024	0.098	0.026	0.245

method (wt loss), PD, and EIS. FTIR was used to examine the products' composition and microstructure. We discussed the kinetic parameters, adsorption mechanism, and adsorption type. SEM was used to examine the carbon steel's corrosion morphology with and without corrosion inhibitors. This work sheds important light on the creation of environmentally friendly corrosion inhibitors for carbon steel.

2. EXPERIMENTAL SECTION

2.1. Preparation of P.cubebaOE. To make the plant extract, the sample was purchased from a local market and ground into a fine powder, yielding 200 g of powdered materials. These were then extracted individually by soaking 500 mL of methanol at room temperature six times. Then, using a rotary evaporator set to 45 °C, the sample's methanolic extract was concentrated to almost dryness under low pressure, yielding a crude methanolic extract that was saved for additional study. After that, the extract was dissolved in 500 mL of ethanol to create a 500 ppm concentration stock, which yielded fictitious inhibitor efficiency values.[35] To prepare the various concentrations used in this study, deionized water was used. The molecular structures of the major constituents in P.cubebaOE, which are caffeic acid, ferulic acid, Gallic acid, syringic acid, (−)-catechin, and rutin, are shown in Figure 1.

2.2. Materials Preparation. Table 1 lists the chemical details of the pieces of C-steel that were used. For the electrochemical measurement studies, coupons with varying dimensions of 2 cm × 2 cm × 0.1 cm and 1 cm × 1 cm × 0.1 cm were formed. To get rid of the grease and dirt, deionized water and alcohol were used to scrub every specimen. Every preparation used deionized water. Sandpaper in a range of sizes was used to polish the samples. For all measurements, a 1.0 M sulfamic acid solution served as the corrosive medium. The *P. cubeba* extract was diluted in 1.0 M H_2NSO_3H corrosion medium to prepare (50, 100, 150, 200, 250, and 300 ppm) test solution, respectively.

2.3. Mass Loss. C-steel specimens with a thickness of 2.0 cm × 2.0 cm × 0.2 cm were used for mass degradation measurements, and they were polished to varying degrees with sanded before being scrubbed with double distilled water, followed by alcohol for eliminating debris and then adequately dried and counted. The weight is then used to calculate WL at (25−45 °C) using standard methods; this data was computed using the formula below.[36−39]

$$\% \text{ IE} = \theta \times 100 = 1 - \frac{W}{W_*} \times 100 \quad (1)$$

The diminution in mass of metal absent from and along with the evaluated extract is shown by W and W^*, consequently.

2.4. Electrochemical Laboratory Tests. Electrochemical laboratory tests were performed using a traditional platinum, calomel, and C-steel three-electrode cell at an average temperature of 25 °C. In this model, the calomel conductor served as an indicator, the platinum-based electrode functioned as a sort of counter electrode, and the C-steel electrode operated as the actual working electrode. The C-steel wire was submerged at a closed loop to attain a semistable condition. In the present situation, impedance was recorded at multiple points, with attribute Hz from 10^{-2} to 10^{-5} Hz, in addition to the presence of intermittent current signals of 5 mV, employing the Gamry Instrumentation category G 750TM -Potentiostat/Galvanostat/ZRA device. To verify the reliability and reproducibility of the measurements of what was executed three times, and all output was gathered.

2.5. Theoretical Calculations. Gaussian 09, Revision A02 was used for the quantum chemical computations.[40] Initially, the inhibitors in the examination were analyzed using molecular mechanics optimization of the conformers to determine which one had the lowest energy. The calculations began without any geometry restrictions and were performed for the neutral species of the molecules under investigation until complete geometry optimization was attained in the ground state. For every optimized structure, the calculated vibrational modes showed no

https://doi.org/10.1021/acsomega.3c09334
ACS Omega 2024, 9, 5024−5037

imaginary frequency. The density functional theory (DFT) approach was used without symmetry constraints and at the 6-31G(d,p) basis-set level. The Becke three-parameter hybrid B3[41] with the L−Y−P (Lee−Yang−Parr) correction functional (B3LYP) was used for all geometry calculations using Gaussian 09.[42] The solvent effect was more accurately represented by the polarized continuum model (PCM).[43] Additionally, using calculation parameters that yield similar results, the DFT scale calculations were performed using the DMol3 module implemented in Materials Studio 7.0 (Accelrys Inc., San Diego, California).[44,45] Using a double numeric plus polarization (DNP) basis set and BLYP functional, the gradient-corrected functional method (GGA) was applied.[46,47] Through COSMO control, the effect of the solvent (aqueous phase) was incorporated into the DMol3 calculations. Other significant quantum parameters were calculated using the obtained quantum chemical parameters, which included the energies of highest-occupied-molecular-orbital (HOMO) and lowest-unoccupied-molecular-orbital (LUMO).[48]

2.6. Quantum Monte Carlo (MC) Simulations. The Materials Studio program, version 7.0 (Accelrys Inc., San Diego, California), was used to run MC simulations in a simulation box with periodic boundary conditions. In order to create a 30 Å vacuum slab, the pure Fe crystal was chosen and split along the plane that required the least amount of energy, which was 110. By lowering its energy, the flat Fe surface of (110) was made more flexible, allowing its surface to expand to a supercell (10/10). Utilizing the MC search in a test box with one molecule of each inhibitor and a simulated corrosive species, the simulation analysis was performed by assigning the high-quality force field known as COMPASS to combine inorganic substances and organic characteristics.[49]

2.7. Surface Characterization. Using a Z-imaging scanning electron microscope (SEM, FEI Inspect S, Oxford) with an X-ray diffractometer and an acceleration beam (25−30) kv. With a vacuum pressure of 60 Pa and spot size (5−6) utilizing a backscattering detector, the C-steel interface was completely screened with respect to its inhibitor- and inhibitor-free variations. Electron beam acceleration for the SEM occurs via 25 kV voltage systems. After going through the electromagnetic lens and apertures, the electron beam becomes narrower. With the aid of scan coils, the beam then scans the metal surface. Following the generation of SEM-type signals from the region of beam and specimen interaction, the C-steel surface was photographed. In the purpose of this research, two C-steel pieces were left submerged for 48 h in sulfamic acid alone (Blank) alongside one in sulfamic acid with 300 ppm of P.cubebaOE blends.[36,37]

2.8. AFM Technique. The AFM approach works well because it can measure the roughness of a variety of surfaces.[50,51] Through the use of AFM, it was possible to gain a clear understanding of the changes in surface shape that occur at a distance of several hundred nanometers because of the development of consumption and the placement of minding successive layers on the metallic substrate when inhibiting agents have been added. The Pico SPM2100 is the AFM device model. An AFM device working in contact mode in the air was used to create images in three and two dimensions at the Nano unit of the College of Engineers at Mansoura University. 5 m × 5 m AFM imagery portions were generated at an average of 2.4 lines per second.

2.9. FTIR Technology Spectra. The spectral data from the P.cubebaOE extract (crude) have been employed with IR affinity (PerkinElmer). They were completed in the university's school of pharmacy's core laboratories at Mansoura Univ.

3. RESULTS AND DISCUSSION

3.1. Mass Loss Method. The inhibition ratios at temperatures between (25 and 45 °C) were obtained using eq 1. The results showed that the values for the CR and % IE of the (P.cubebaOE) extract were established. The results are presented in Table 2 and Figure 2. The results showed that increasing the amount of (P.cubebaOE) extract increases the inhibition ratios, which were found to decrease as the temperature increased. This happens as a result of the plant extract desorbing from the metal's surface. 300 ppm was found to be the ideal concentration for the inhibition process, resulting in a maximum inhibition rate of 96%. These results enable us to conclude that this plant extract has a high level of effectiveness in preventing C-steel corrosion in a 1.0 M H_2NSO_3H solution.

Table 2. Several Measures of Inhibition for 1 M H_2NSO_3H's Corrosive Effects on C-Steel at Various Concentrations, Both with and without P.cubebaOE

C., ppm	k_{corr}, mg cm^{-2} min^{-1}	% IE
50	0.0203	85.6
100	0.0025	87.7
150	0.0020	89.7
200	0.0016	92.0
250	0.0012	93.8
300	0.00083	96.0

3.2. Adsorption Isotherm. Thermal isotherms determine that the corrosion process is essentially dependent on the surface coverage Θ, which means that it is a further part of the IE, where Θ = IE/100. One of the most useful tools for quantitatively expresses adsorption that describes the metal/inhibitor/environment system is the adsorption isotherm. The data was analyzed using standard adsorption isotherms such as Langmuir, Freundlich, Temkin, and Flory-Huggin Frumkin. The results of our experiment in this study showed that the Langmuir isotherm fit the data. Plotting C/Θ against C at 25 °C for P.cubebaOE, as indicated by eq 2, with a slope of 1 and an intercept of k_{ads}, is illustrated in Figure 3. The straight lines in this plot show that the Langmuir isotherm is followed by P. cubebaOE adsorption on the C-steel surface. After multiple attempts to adopt a relationship between the greatest concentration of the inhibitor at a given temperature and the degree of surface coverage, the Langmuir adsorption isotherm was shown to be the best curve to characterize the inhibitory performance. The equation[52,53] below summarizes the idea that, in the case of the plant extract, the metallic surface contains a specific number of adsorption cores and that each center contains a specific type of adsorbent.

$$\frac{C}{\theta} = \frac{1}{K_{ads}} + C \tag{2}$$

The net energy ΔG°_{ads} was derived using the formula after the adsorption factor K_{ads}' quantity had been established.

$$K = \frac{1}{55.5}\exp^{-\Delta G_{ads}/RT} \tag{3}$$

The level of concentration of water on the metal surface is 55.5 in mol/L. The distributions of ΔG_{ads}° as a reflection of temperature are shown in Table 3 at an average temperature around 298 and 318 K. As a direct consequence of the findings,

https://doi.org/10.1021/acsomega.3c09334
ACS Omega 2024, 9, 5024−5037

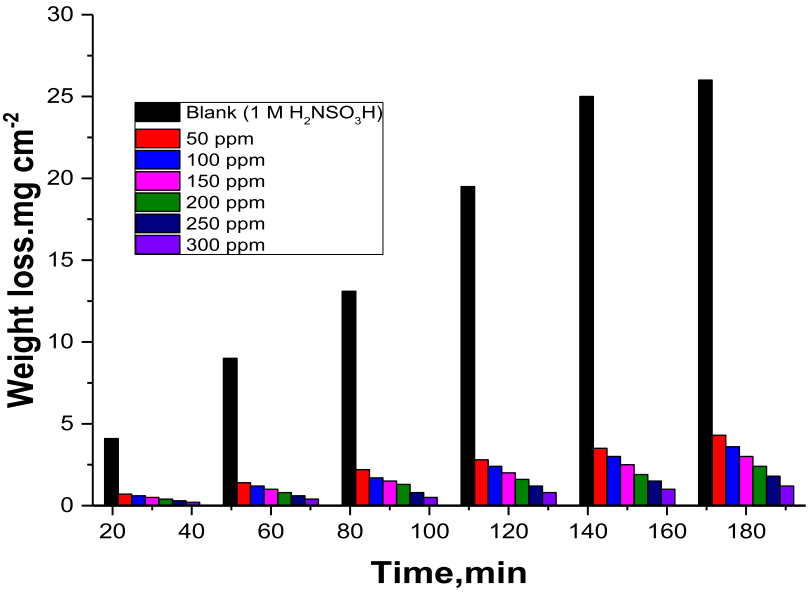

Figure 2. Impact of submerged intervals on the amount of mass loss of C-steel in 1 M H_2NSO_3H containing and not containing varied P.cubebaOE doses at 25 °C.

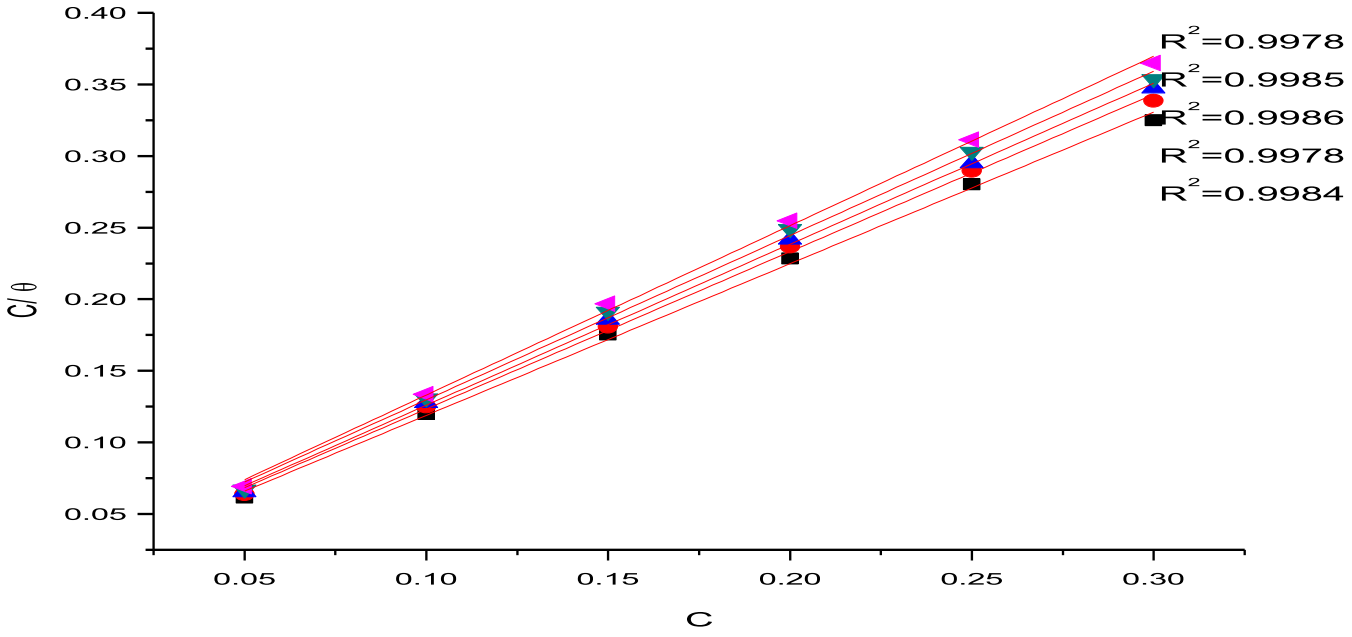

Figure 3. Langmuir pattern produced by P.cubebaOE for rusting of C-steel in 1 M H_2NSO_3H solution at 25 °C as C/vs C, M.

Table 3. Data of P.cubebaOE Adsorption at Multiple Temperatures on a C-Steel Outer Layer in 1 M H_2NSO_3H

temperature, °C	$K_{ads} \times 10^{-3}$ M^{-1}	$-\Delta G^{\circ}_{ads}$ kJ mol^{-1}	ΔH°_{ads} kJ mol^{-1}	ΔS°_{ads} J mol^{-1} K^{-1}
25	2.02	15.32	118.60	44.2
30	1.96	15.60		48.90
35	1.93	21.00		65.05
40	0.98	21.14		68.62
45	0.940	21.50		68.79

we derived an association between $\Delta G_{ads}{}^{\circ}$ and T, which means that $\Delta G_{ads}{}^{\circ}$ is strongly influenced by temperature. This formula[S4] can be used to compute the entropy (ΔS_{ads}) and enthalpy of Adsorption capacities (ΔH_{ads})

$$\Delta G^{\circ}_{ads} = \Delta H^{\circ}_{ads} - T\Delta S^{\circ}_{ads} \quad (4)$$

The negative $\Delta G_{ads}{}^{\circ}$ values increased with the increase of % IE values, which confirm the stability of the adsorbent layer physical adsorption, can indicate the extract's spontaneous sorption on the outer layer that covers C-steel. We discover that as $\Delta G_{ads}{}^{\circ}$ increases, the values of the inhibition ratios rise as well, and as ΔH_{ads} has a sign that is negative, we infer that the adsorption of the extract on the surface of the C-steel is an exothermic operation, meaning that % IE decreases as temperature rises. On the other hand, the rise in solvent entropy when disorder develops at the metal/solution interface is what is responsible for the positive value of $\Delta S_{ads}{}^{\circ}$. This is a result of P.CubebaOE molecules dislodging H_2O molecules from the metal surface in the test medium.

https://doi.org/10.1021/acsomega.3c09334
ACS Omega 2024, 9, 5024−5037

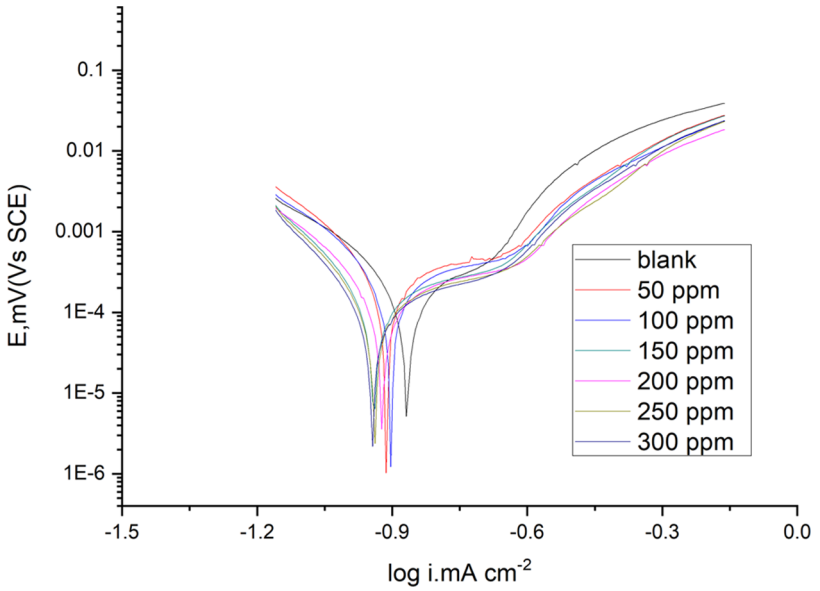

Figure 4. Illuminates the potentiodynamic polarization diagrams for C-steel dissolving in 1 M H_2NSO_3H in both the existence and nonexistence of a variety of P.cubebaOE at 25 °C.

Table 4. Illustrates the Corrosive Potential (E_{corr}), Corrosive Density of Current (i_{corr}), the Tafel Slopes (a, c), Degree of Surface Coverage (θ), and the Inhibition Effectiveness (% IE) of C-Steel for P.cubebaOE in 1 M H_2NSO_3H at 25 °C

inhibitor	C., ppm	$-E_{corr}$ mV vs SCE	$I_{corr} \times 10^{-4}$ μA cm^{-2}	β_a, mV dec^{-1}	$-\beta_c$, mV dec^{-1}	% IE
blank	0	867	301.0	366	390.0	0.0
P.cubebaOE	50	847	173.0	319	281	42.5
	100	852	149.0	277	250	50.4
	150	742	69.7	340	130	76.8
	200	938	47.8	82	93	84.1
	250	854	39.7	157	59	86.8
	300	552	25.8	64	57	91.4

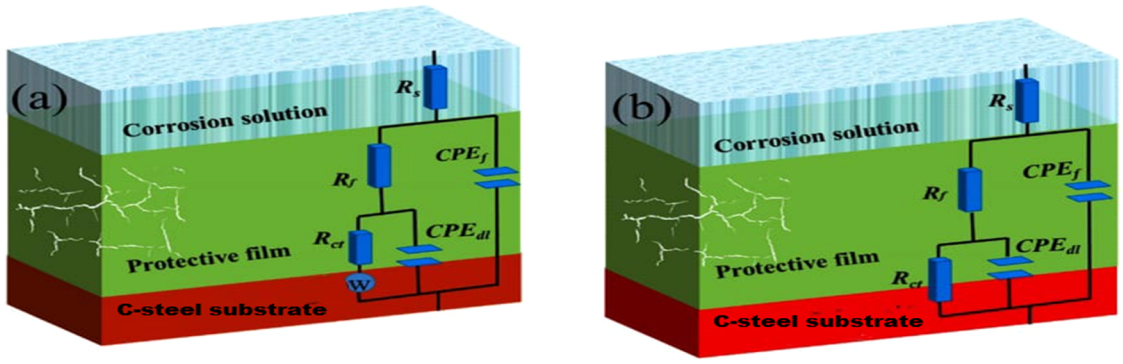

Figure 5. Modeling a similar circuit to match a laboratory EIS.

Table 5. P.cubebaOE Doses with and without Respect to the Kinetics of the C-Steel Electrochemistry in H_2NSO_3H

inhibitor	C., ppm	Y_o, $\mu\Omega^{-1}$ s^{n}cm^{-2}	R_{ct}, Ω cm^2	$C_{dl} \times 10^{-4}$, μF cm^{-2}	θ	% IE	$X^2 \times 10^{-3}$
blank	0	102	110.5	9.77	0.0	0.0	13.5
P.cubebaOE	50	81	339.7	8.03	0.674	67.4	20.1
	100	79	498.5	3.91	0.778	77.8	17.2
	150	71	544.5	3.62	0.797	79.7	15.6
	200	61	1219	0.231	0.909	90.9	15.8
	250	40	1397	0.129	0.921	92.1	16.9
	300	35	1492	0.112	0.926	92.6	14.9

3.3. Potentiodynamic Polarization (PDP) Tests. Figure 4 displays the PDP bends of C-steel in 1 M H_2NSO_3H attendance and the absence of changed doses of P.cubebaOE. Table 4 lists the electrochemical properties, such as current density (ic_{orr}),

https://doi.org/10.1021/acsomega.3c09334
ACS Omega 2024, 9, 5024−5037

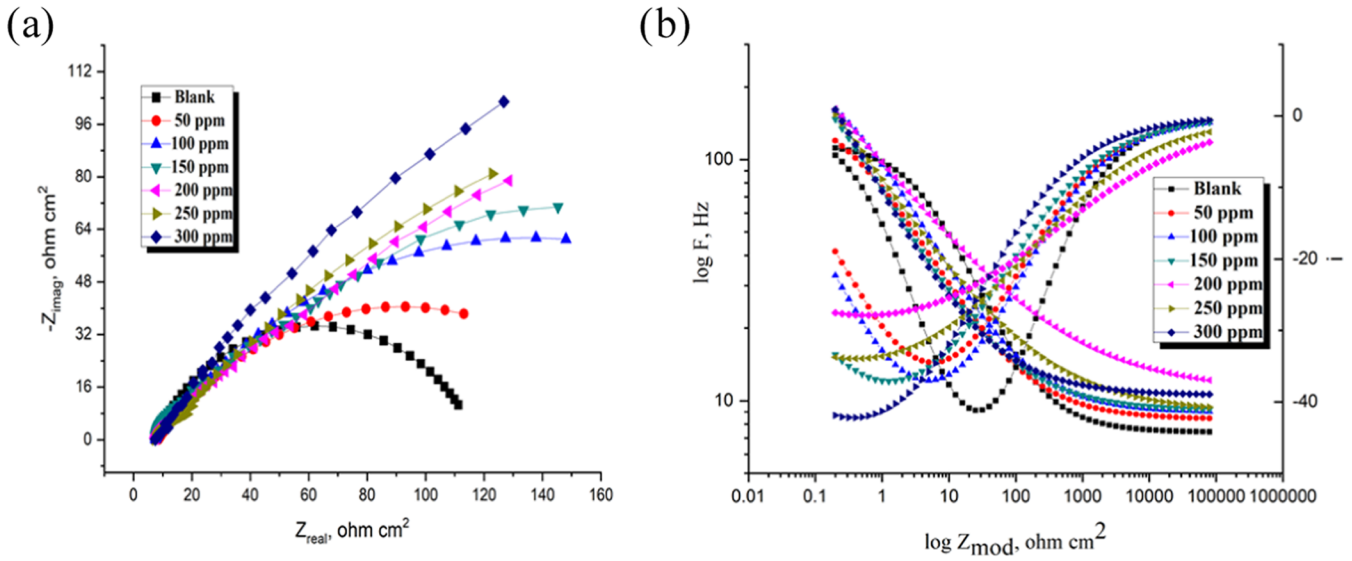

Figure 6. Panels (a, b) show the Nyquist and Bode plots for the corrosion of C-steel in 1 M H_2NSO_3H in both the absence and the existence of multiple amounts of P.cubebaOE at 25 °C.

corrosion potential (E_{corr}), and anodic (β_a) and cathodic (β_c) slopes, that were derived by Tafel extrapolation at the corrosion potential. It has been noted that i_{corr} diminishes as the inhibitor concentration is increased. IE % and (θ) were calculated using the polarization curves (eqs 5 and 6)

$$\text{IE } \% = 1 - \frac{i_{corr}}{i^{o}_{corr}} \tag{5}$$

$$\theta = \text{IE}\%/100 \tag{6}$$

where the current corrosion densities of chemicals are represented by the variables $i_{corr}{}^{o}$ and i_{corr}, respectively. The polarization resistance (R_p) of the test specimens in the 1 M H_2NSO_3H solution was calculated using the Stern−Geary eq 7 below, taking into account the presence or absence of P.cubebaOE inhibitor.[27]

$$R_p = \beta a \beta c / 2.303\, i_{corr}(\beta a + \beta c) \tag{7}$$

At 25 °C, the highest inhibition effectiveness of 91.4% was obtained with additions of 300 ppm of the examined corrosion inhibitors, P.cubebaOE. It is evident that the effectiveness of inhibition steadily improves as the inhibitor dose increases. As the dosage of the corrosion inhibitor is increased, i_{corr} significantly drops and reaches a minimum of 25.8 μA cm^{-2}. These results validate the examined extract's excellent inhibition and film-forming capacity.[27] The addition of P.cubebaOE to the 1 M H_2NSO_3H solution does not change the hydrogen evolution mechanism or the reduction of H^+ ions at the C-steel surface, which mostly occurs through a charge-transfer mechanism,[55−57] based on the parallel cathodic Tafel lines. Depending on whether the inhibitor causes a shift in corrosion-free potential E_{corr} that is larger than 85 mV of SCE in either direction after being added, the inhibitor can be classified as either cathodic or anodic. If not, it is believed that the inhibitor affects both processes. After the addition of the corrosion inhibitor, the overall change in E_{corr} in this experiment was determined to be minimal or less than 85 mV. Since the inhibitor suppresses both the anodic and cathodic processes,[58] this proves that it is a mixed-type inhibitor. The anodic reaction is predominant, although the inhibitor is a mixed inhibitor, as indicated by the positive E_{corr} displacement. The inhibitory characteristics of the inhibitors under study at the highest doses are indicated by the % IE values shown in Table 4. The outcomes of the MR and EIS measurements agree well with these findings.

3.4. Electrochemical Impedance Spectroscopy (EIS) Tests. EIS studies provide details about the kinetics of the electrode processes and the surface properties of the systems being studied. Information can be obtained from the shape of the impedance diagram.[59] After immersing the steel for 30 min at 25 °C in a 1 M H2NSO3H solution with and without varying inhibitor concentrations, the corrosion efficiency of the steel was evaluated using the EIS method. attempting to take into consideration for all of the processes involved in the electrical response of the system, Figure 5 shows an equivalent circuit that is a parallel combination of the charge-transfer resistance (R_{ct}) and the constant phase element (CPE), both in series with the solution resistance (R_s). The CPE element offers an explanation for the depression of the capacitance semicircle, which is attributed to surface heterogeneity caused by impurities, dislocations, grain boundaries, inhibitor adsorption, and the formation of porous layers.[60] The impedance of the CPE is represented by the following equation

$$C_{dl} = Y_O(\omega_{max})n - 1 \tag{8}$$

where, n ($-1 < n < 1$) is the deviation index, ω is the angular frequency, and Y^o is the CPE constant. The non-uniform distribution of current due to oxide surface flaws and roughness appears to be linked to the "n" values. While real capacitive behavior is extremely uncommon, CPE is the ideal capacitor for $n = 1$. "n" values close to 1 indicate the deviation from the ideal capacitor (Table 5). A constant phase element (CPE) was utilized for data fitting rather than an ideal capacitor; the capacitance was calculated using the value obtained from the data fitting because the "n" values obtained were within the range of 0.9. The fit quality to the analogous circuit was assessed using the chi-square value.[61] The obtained chi-square values (0.0000135−0.000201) from Table 5 show that the suggested circuit fits the data well. Figure 6a,b shows the Nyquist and Bode graphs of the systems under study, respectively. In 1 M H_2NSO_3H solution, for the P.cubebaOE under examination, it is

https://doi.org/10.1021/acsomega.3c09334
ACS Omega 2024, 9, 5024−5037

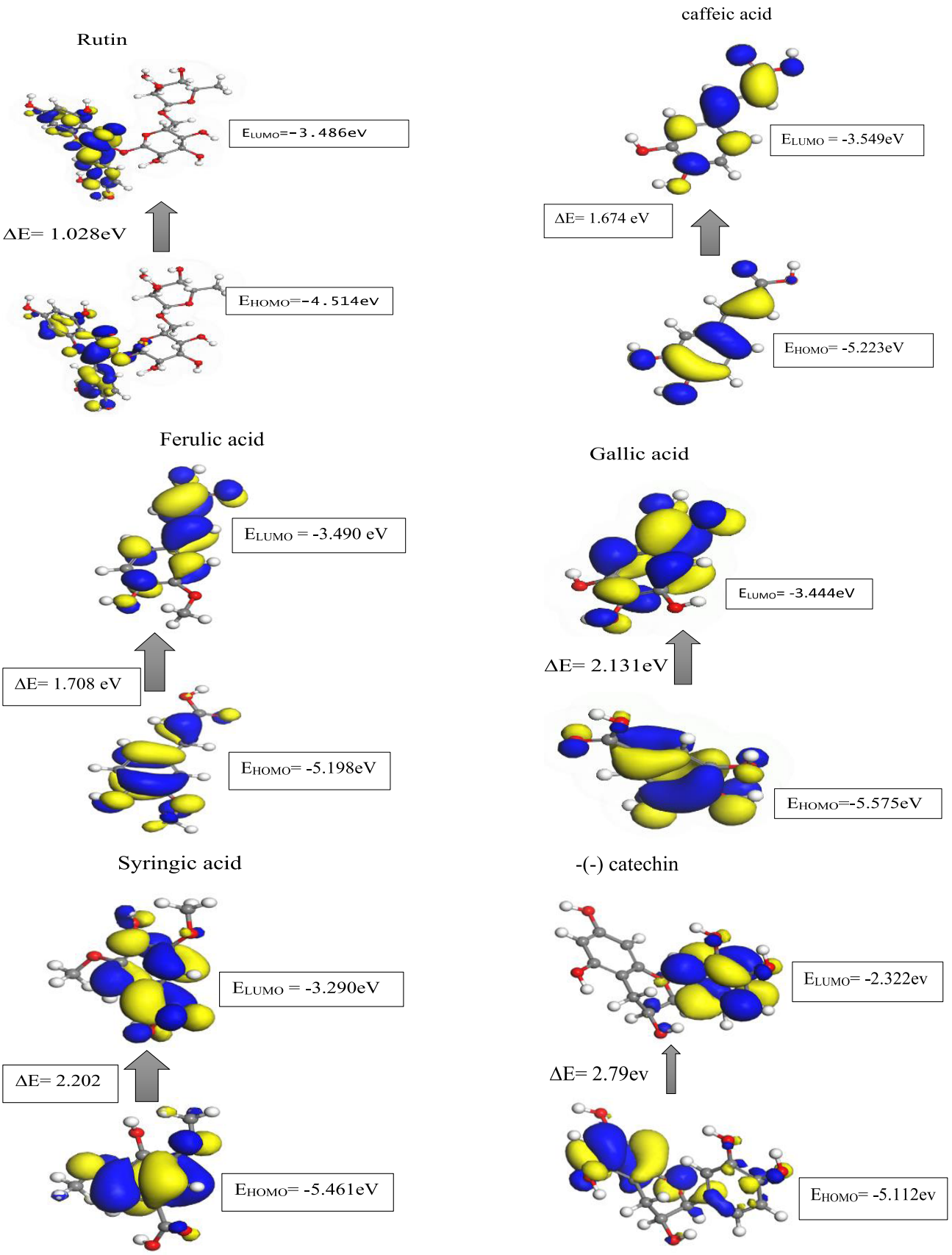

Figure 7. HOMO and LUMO molecular orbitals of major ingredients of P.cubebaOE.

clear from Figure 6 that the C-steel displayed typical impedance behavior. The frequency dispersion caused the Nyquist graph of C-steel metal in 1 M H_2NSO_3H solution to stray from the perfect circular shape.[61] The capacitive loop diameter noticeably

https://doi.org/10.1021/acsomega.3c09334
ACS Omega 2024, 9, 5024−5037

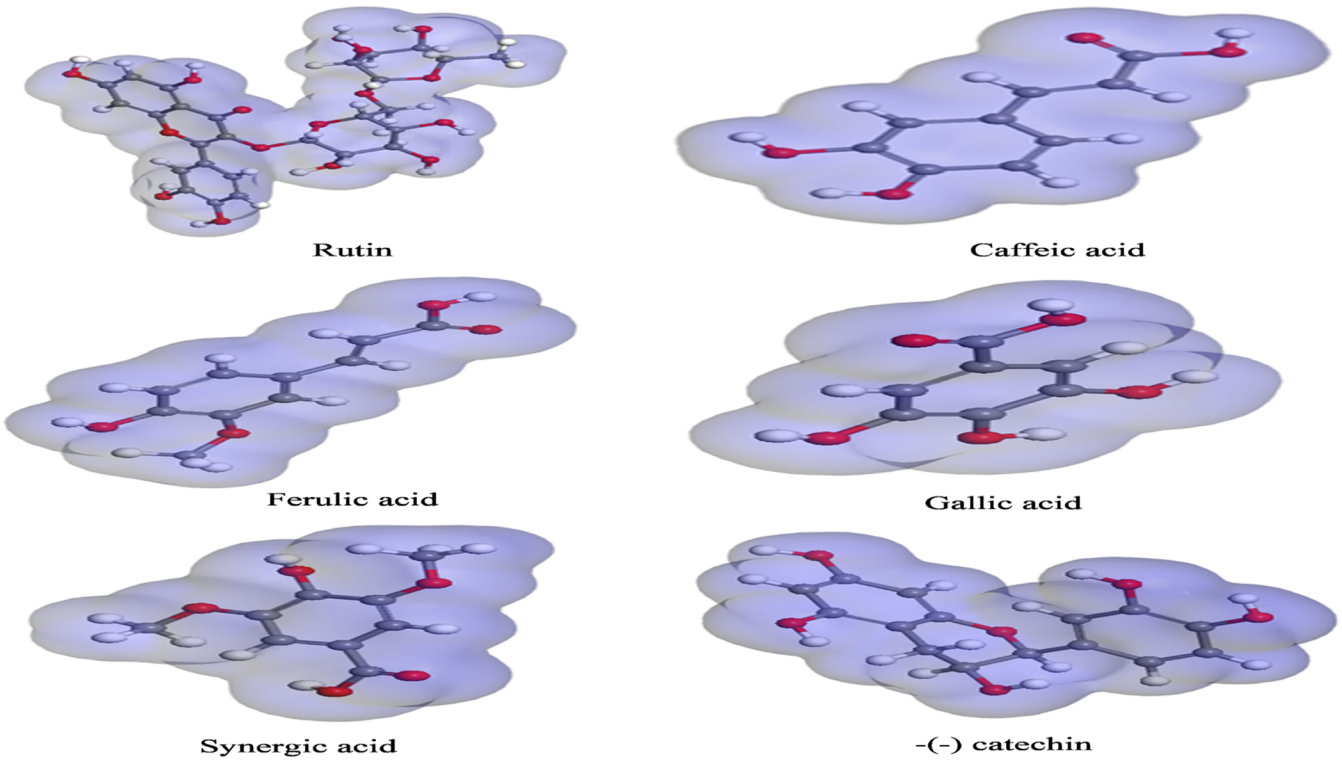

Figure 8. ESP Pictures of P.cubebaOE.

Table 6. P.cubebaOE Compound Adsorption Characteristics from Monte Carlo Simulation on Fe(110) Surface

structure	total energy	adsorption energy	rigid adsorption energy	deformation energy	E_{ads}: compound
Fe(110) -1 rutin	−2524.269	−2567.303	−2676.787	109.48362879	−106.09305624
Fe(110) -1 caffeic acid	−2602.874	−25194.88	−26403.60	120.87228885	−125.23564903
Fe(110)-1 ferulic acid	−2646.979	−2582.141	−2702.923	120.78118244	−135.73621684
Fe(110)-1 gallic acid	−2563.120	−2538.716	−2661.619	122.90336020	−117.54093563
Fe(110) -1-(−) catechin	−2568.665	−2540.818	−2664.544	123.72645644	−44.24846043
Fe(110)-1 syringic acid	−2514.338e	−2523.172	−2643.922	120.75000213	−94.10524621

increases upon the addition of the P.cubebaOE extract to the 1 M H_2NSO_3H solution. The inhibitor either adsorbs on the surface of Fe or thin films begin to form there as the concentration increases. This protective layer lowers the active surface area of Fe and enhances its corrosion resistance behavior, thereby significantly slowing down the corrosion of C-steel in a 1 M H_2NSO_3H solution. It is noteworthy that the profile of the impedance behavior remained unchanged when the concentration of the inhibitors under investigation was changed, indicating a similar mechanism for these inhibitors' corrosion inhibition of C-steel. According to this, in the absence of inhibitors, the Nyquist plot for C-steel metal shows a slightly depressed semicircular pattern, suggesting that the charge-transfer mechanism is primarily responsible for controlling C-steel metal corrosion in the 1 M H_2NSO_3H solution.[62] In Figure 6b, two temporal constants are displayed. The first one first appears in the middle-frequency range and is related to the capacitive loop of the oxide layer on the C-steel surface. The second time constant that appeared in the low-frequency region is caused by the inductive loop that results from the relaxation process of the adsorbed inhibitor molecules on the surface of C-steel or the redissolution of the Fe + 2 oxide layer surface.[63] The semicircle's diameter grew as the studied inhibitors were added to the solution, delaying the corrosion of the C-steel by raising R_p, the polarization resistance, and lowering CPE values. Therefore, lower CPE values and higher R_p values were linked to the examined extract's effectiveness. As the concentration of the inhibitor increased, this increase became more noticeable, indicating that the inhibitors had adhered to the surface of the C-steel specimen. Bode graphs show the same patterns of activity. The capacitance loop was identified as the characteristic with a single time constant from the Bode plots. These findings imply that when P.cubebaOE is present, C-steel resists corrosion more effectively. Charge-transfer resistance (R_{ct}), double-layer capacitance (C_{dl}), Y° (CPE), n, quality of fit (χ^2), and percentage η_{EIS} are among the impedance metrics that are listed in Table 5. Double-layer capacitors with some holes are represented by the CPE and their n values.[64] A decrease in the local dielectric constant and/or an increase in the double layer's thickness caused the Y° (CPE) values to decrease as the concentration of inhibitors increased. This indicated that the inhibitor molecules prevented the corrosion of C-steel by adsorbing at the Fe/H_2NSO_3H interface. The fact that the R_{ct} values increased as the inhibitor concentration increased and remained higher than when it was absent suggests that these additives are adsorbed on the C-steel surface and form a protective layer. This layer acts as a barrier to the transfer of charge and mass.[65] As the inhibitor concentration increased as the additive concentration was raised, the C_{dl} values dropped.[66]

The following equation was used to determine the C_{dl} value[67]

https://doi.org/10.1021/acsomega.3c09334
ACS Omega 2024, 9, 5024−5037

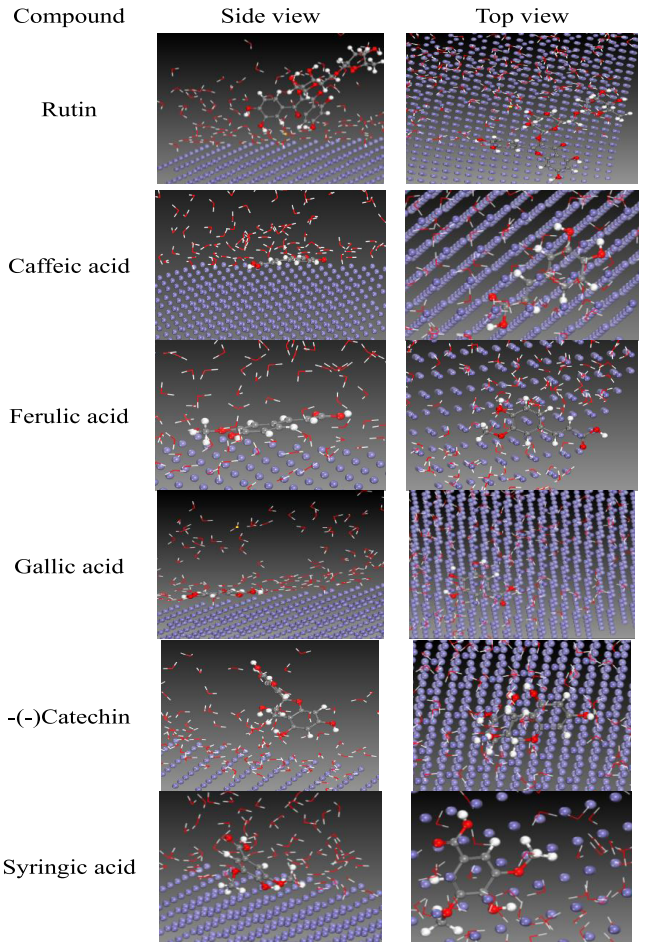

Figure 9. Adsorption of P.cubebaOE compounds on the Fe surface.

$$C_{dl} = \frac{1}{2\pi f \ \max R_{ct}} \tag{9}$$

Using the following equation

$$\%\ \eta\ \text{EIS} = \frac{R_{ct} - R_{ct}^{*}}{R_{ct}} \tag{10}$$

The corrosion percentage η was calculated, where R_{ct}* is the charge-transfer resistance without the inhibitor and R_{ct} is the charge-transfer resistance with the inhibitor. η% rises as a result of additions creating an adsorbed layer on the C-steel surface. This layer thickens with an increase in additive concentration.[68] Furthermore, the inhibitory efficiency obtained from the EIS study was comparable to those of the WL and PDP tests.

3.5. Molecular Modeling. *3.5.1. HOMO–LUMO Molecule Orbital.* The LUMO and HOMO density profiles of the studied chemicals in the aqueous phase are shown in Figure 7. It demonstrates that green has a low electron density, whereas red has a high electron density. In situations where there is a high electron density, the metal surface can donate electrons. In the green area, electrons are attracted to the metal surface. The distribution of these two locations plays an important role as resonance is mainly caused by the bonds between the oxygen and nitrogen atoms on the benzene ring. The center of the LUMO in the meanwhile is made up of carbon atoms. *E* values that are lower may be an indication of improved inhibitory efficiency. The *E* value can be used to assess how reactive the inhibitor molecule is to the metal atom. Reduced *E* values could

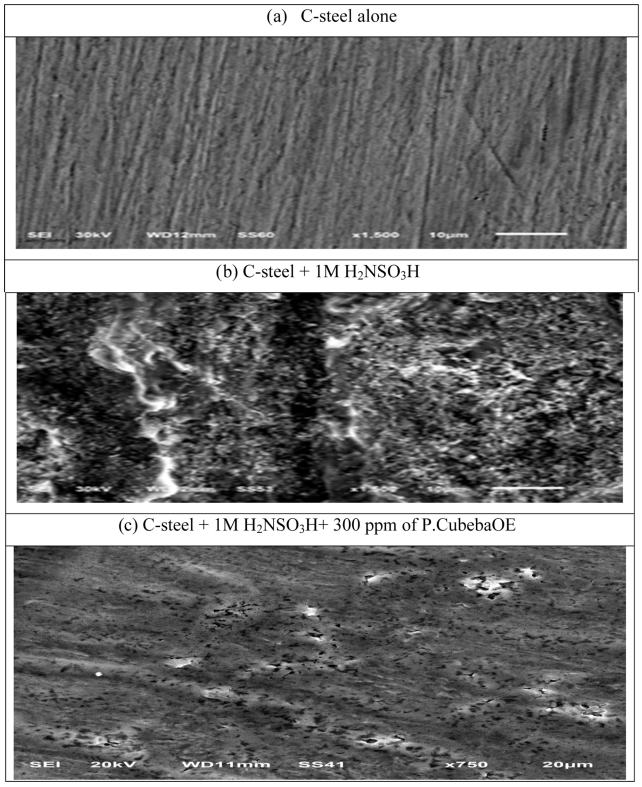

Figure 10. SEM image of pure C-steel in 1.0 M H_2NSO_3H solution (a), without P.CubebaOE at the optimal concentration (b), and with P.CubebaOE present (c).

be a sign of more effective inhibition. The inhibitor molecule's reactivity with the metal atom can be evaluated using the *E* value. The most stable is − (−) catechin (E = 2.79), according to the DFT simulations (Figure 8).

3.5.2. 2D Maps of Electrostatic Potential. The distribution of electrons and, subsequently, where they are concentrated within each molecule can be seen by using ESP maps. According to the electron density contour maps, oxygen atoms on the examined molecule inhibitor appear to be favorable interaction locations, which is consistent with the different functions of oxygen and the other atoms. A dark red outline surrounds the contact regions that offer the bonding contacts between the inhibitor and metal surfaces. ESP maps can be used to observe the distribution of electrons and, consequently, where they are concentrated within each molecule.

3.5.3. Monte Carlo (MC) Simulation. MC simulation is a perfect simulation method to find the most stable adsorption conformations in 1 M H_2NSO_3H of P. cubebaOE. Table 6 contains a list of the simulation results for the examined extract, which are displayed in Figure 9. The ideal arrangement of the adsorbed molecules on Fe (110)'s metal surface is seen in Figure 9. The inhibitory molecules, which are abundant in electrons, cause the molecules listed to be adsorbed on the metal's surface from the motive. Table 6 compiles the values of the inhibitors' energetic ratios (dE_{ads}/E_{Ni}), rigid energy (E_{rigid}), deformation energy (E_{def}), and adsorption energy (E_{ads}). These values indicate the established interactions between the occupied orbitals of the studied derivatives and the unoccupied orbitals of Fe(110). These inhibitory structures act as active voltages according to the research. When two materials are combined during the adsorption process, which involves the bonding of an electron, ion, or molecule (adsorbent) to the solid surface,

https://doi.org/10.1021/acsomega.3c09334
ACS Omega 2024, 9, 5024−5037

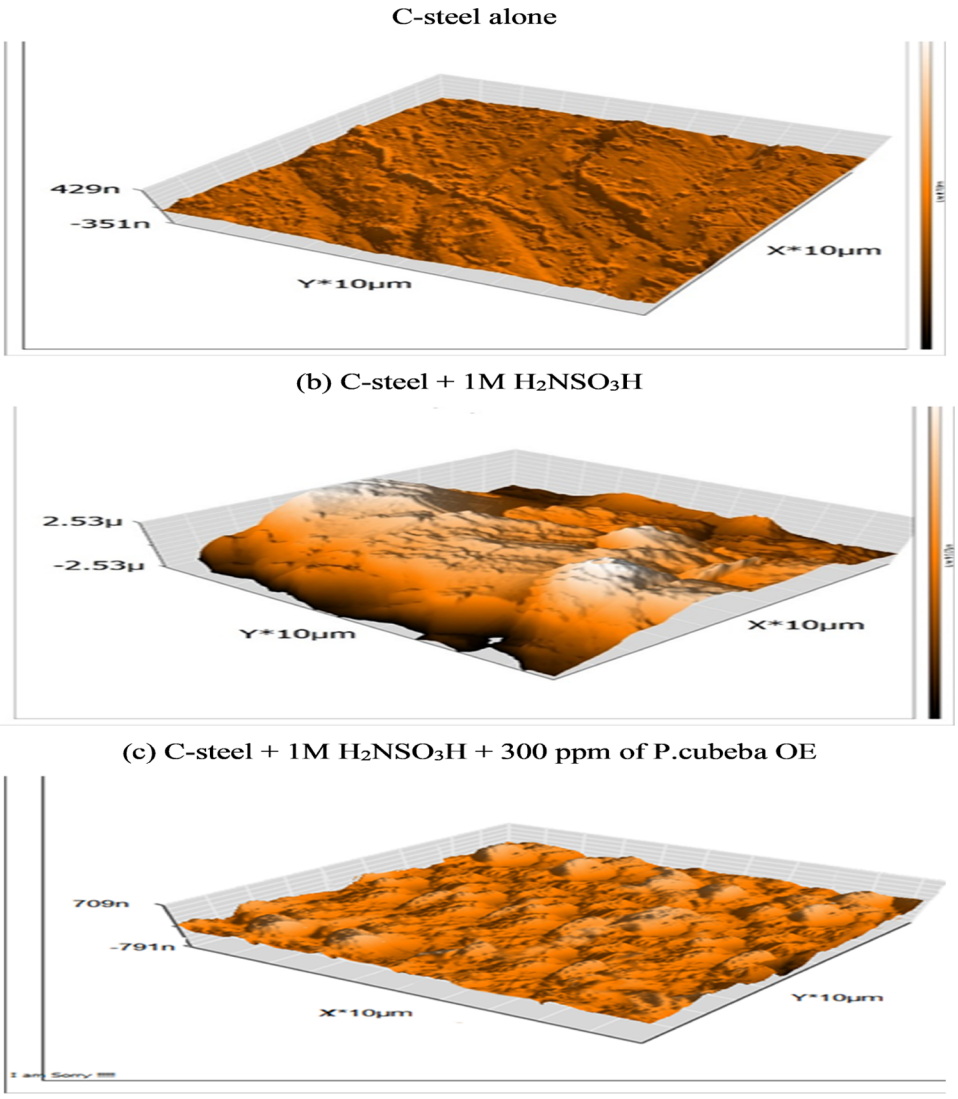

Figure 11. AFM image of pure C-steel (a) and steel that has been submerged in 1.0 M H_2NSO_3H solutions without P.CubebaOE (b) and with it (c), respectively.

Table 7. AFM Parameters of P.CubebaOE Compounds

sample	RMS roughness (S_q), nm	mean roughness (S_a), nm
a	21.67	16.74
b	1254.8	995.72
c	289.82	183.60

adsorption energy is defined as decreasing energy.[69] These derivatives prevent corrosion on the C-steel.

3.6. SEM Examination. SEM research has verified the P.cubebaOE layer's adsorption on the surface of C-steel. Figure 10a−c depicts SEM images of the C-steel's surface before and after 48 h of immersion in 1 M H_2NSO_3H with a dosage of 300 ppm of P.cubebaOE. Without having P.cubebaOE, H_2NSO_3H corrosion has clearly harmed the C-steel surface, but the metallic edge is still discernible (Figure 10b). The metal surface, in variance with the material under assessment, appears not to rust (Figure 10c). It was found that the extract created a slight film on the C-steel's outside that restricted corrosion.[70]

3.7. Atomic Force Microscopy (AFM). The 3D picture of the C-steel indicates that, in the absence of the P.CubebaOE inhibitor under investigation, the metal surface of the steel has allegedly been repeatedly corroded by the corrosive attacks of 1 M sulfamic acid (Figure 11b). However, the 3D images (Figure 11c) indicate that the aggressive solution has smoother surfaces than the blank, indicating that the addition of an inhibitor reduces C-steel corrosion. The average RMS roughness (S_q) and mean roughness (S_a) of the films produced on the C-steel surface by using the Gwyddion modular program are displayed in Table 7. The data in Table 7 indicate that the compound is effective in protecting the surface of C-steel from corrosive media because the RMS roughness and mean roughness of the blank are higher than those of the inhibitor under study and pure metal. The sequence of inhibitory efficacy found by weight loss research and electrochemical tests is supported by additional data from the AFM.

3.8. Fourier Transform Infrared Spectroscopy (FTIR) Studies. Figure 12 confirms that "the −C═O stretching frequency occurs at 1640 cm^{-1}, with the acute one at 1608 cm^{-1} referring to −C═C stretching, the O−H stretching has changed from 3225 to 3365 cm^{-1}, and the −C═C stretching frequency shifts from 1647 to 1640 cm^{-1} in the film generated on the C-steel submerged in sulfamic acid. The alterations in the IR spectra hint that the bonding of P.cubebaOE with C-steel was

https://doi.org/10.1021/acsomega.3c09334
ACS Omega 2024, 9, 5024−5037

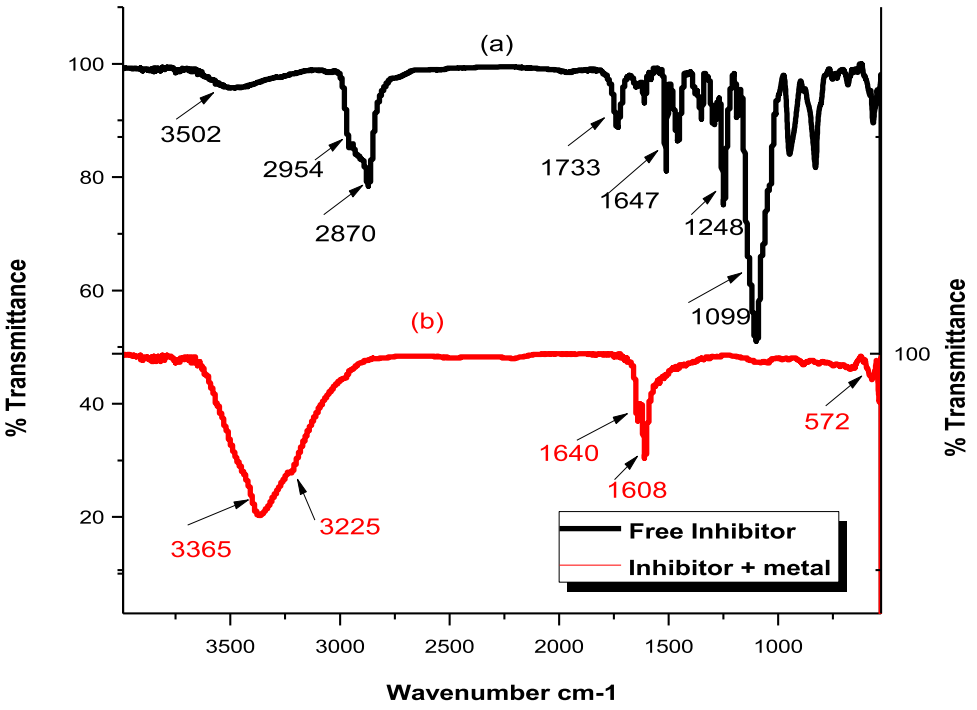

Figure 12. FTIR spectra of P.cubebaOE.

Table 8. Comparison of P.CubebaOE with Some Other Studied (% IE Is Reported at the Maximum) Extracts

source of extract	test medium	metal/alloy	% IE	references
olive leaf extract	H_2NSO_3H	C-steel	89.6	71
Citrus sinensis extract	H_2SO_4	C-steel	83.6	72
aqueous extract of juniperus	H_2NSO_3H	C-steel	72.6	73
tragia involucrata	HCl	C-steel	88.0	74
myrtus communis extract	H_2NSO_3H	C-steel	>85.0	75
P. cubeba official extract	H_2NSO_3H	C-steel	96.0	our results

accomplished through groups of functions that had already existed in it.

3.9. Mechanism of the Corrosion Inhibitors Interaction. The results of the electrochemical experiment show that the P.cubebaOE inhibitor performs exceptionally well at inhibiting corrosion with an efficiency of up to 96.0%. The Langmuir isotherm adsorption model is determined through calculation to be appropriate for this system. The estimated value of ΔG°_{ads} is 20.0 kJ/mol. By using the adsorption technique, P.cubebaOE has demonstrated a protective effect against the corrosion of C-steel in 1 M sulfamic acid solution. The interaction of donor and acceptor molecules between the P.cubebaOE electrons and vacant *d* orbitals on the C-steel surface or the interaction of heteroatoms in the inhibitor with the unoccupied *d*-orbital of the C-steel surface could have defined the mechanism of corrosion inhibition. Adsorption can be broadly classified into three types: chemisorption, physisorption, and retirodonation. Reterodonation is the interaction of pi electrons from unsaturated carbon vacant *d* orbitals of the steel surface with heteroatoms present in the inhibitor and the unoccupied *d*-orbital of the surface from Fe^{2+}. Numerous scientists have looked into the ability of various plant extracts to prevent corrosion under acidic conditions at varying concentrations. According to these investigations, plant extracts with higher quantities demonstrated good corrosion inhibition qualities when used as inhibitors in mildly acidic environments. We examined P.cubebaOE anticorrosive qualities in a 1 M sulfamic acid solution in this investigation. Additionally, we employ plant waste, which is a cost-effective and environmentally responsible choice. A comparison between our studied plant and several of the published plant-based inhibitors is provided in Table 8.

4. CONCLUSIONS

The official extract of piper cubeba was utilized in this study to prevent corrosion in the C-steel while it was submerged in an acidic electrolyte (1 M sulfamic acid). By using computational approaches, EIS and polarization techniques, and gravimetrical calculations, we assessed the corrosion inhibition properties of P.cubebaOE were assessed. According to the results of the electrochemical test, P.cubebaOE inhibition efficiency increased dramatically with the addition of more inhibitor concentrations, reaching a maximum value of 96.0% in the presence of 300 ppm after the working electrode was submerged in the H_2NSO_3H solution for two hours with a mixed-type inhibition behavior. The working electrode surface was shielded from corrosive attacks by a protective coating that was created by the adsorption of P.cubebaOE based compounds on the immersed electrode surface, as shown by the results of the SEM and AFM experiments.

■ ASSOCIATED CONTENT

Data Availability Statement

The authors confirm that the data supporting this study are available.

■ AUTHOR INFORMATION

Corresponding Authors

Aya. M. Salem − *Department of Basic Science, Higher Institute of Electronic Engineering (HIEE), Belbis 44621, Egypt;*

https://doi.org/10.1021/acsomega.3c09334
ACS Omega 2024, 9, 5024−5037

orcid.org/0000-0003-0675-5191; Email: ayasalem993@gmail.com

Merfat S. Al-Sharif − *Department of Chemistry, College of Sciences, Taif University, Taif 21944, Saudi Arabia*; Email: m.alshareef@tu.edu.sa

Complete contact information is available at: https://pubs.acs.org/10.1021/acsomega.3c09334

Author Contributions

M.S.A.-S. contributed to conceptualization, methodology, project administration, and funding acquisition. A.M.S. contributed to software, validation, and formal analysis; writing, editing and data analysis; and supervision. All authors have read and agreed to the published version of the manuscript.

Funding

The researchers would like to acknowledge the Deanship of Scientific Research, Taif University for funding this work

Notes

The authors declare no competing financial interest.

■ ACKNOWLEDGMENTS

The researchers would like to acknowledge the Deanship of Scientific Research, Taif University, for funding this work.

■ REFERENCES

(1) Umorena, S. A.; Obota, I. B.; Ebensob, E. E.; et al. Studies on the inhibitive effect of exudate gum from Dacroydes edulis on the acid corrosion of aluminium. *Port. Electrochim. Acta* **2008**, *26* (2), 199−209.

(2) Jones, D. A. *Princ. Prev. Corros.*, 2nd ed.; Pretice Hall. Inc: Unites States of America, 1996; Vol. 2, p 168.

(3) Jones, D. A. *Princ. Prev. Corros.*, 2nd ed.; Pretice Hall. Inc: Unites States of America, 1996; Vol. 2, p 168.

(4) Raja, P. B.; Sethuraman, M. G. Natural products as corrosion inhibitor for metals in corrosive media−a review. *Mater. Lett.* **2008**, *62* (1), 113−116.

(5) Igual Muñoz, A.; García Antón, J.; Guiñón, J.; et al. Inhibition effect of chromate on the passivation and pitting corrosion of a duplex stainless steel in LiBr solutions using electrochemical techniques. *Corros. Sci.* **2007**, *49* (8), 3200−3225, DOI: 10.1016/j.corsci.2007.03.002.

(6) Orubite, K.; Oforka, N. Inhibition of the corrosion of mild steel in hydrochloric acid solutions by the extracts of leaves of Nypa fruticans Wurmb. *Mater. Lett.* **2004**, *58* (11), 1768−1772.

(7) Oguzie, E. E. Corrosion inhibition of aluminium in acidic and alkaline media by Sansevieria trifasciata extract. *Corros. Sci.* **2007**, *49* (3), 1527−1539.

(8) Chauhan, L.; Gunasekaran, G. Corrosion inhibition of mild steel by plant extract in dilute HCl medium. *Corros. Sci.* **2007**, *49* (3), 1143−1161.

(9) El-Etre, A.; Abdallah, M.; El-Tantawy, Z. Corrosion inhibition of some metals using lawsonia extract. *Corros. Sci.* **2005**, *47* (2), 385−395, DOI: 10.1016/j.corsci.2004.06.006.

(10) Mangale Sapana, M.; Chonde Sonal, G.; Raut, P. Use of Moringa oleifera (drumstick) seed as natural absorbent and an antimicrobial agent for ground water treatment. *Res. J. Recent Sci.* **2012**, *1* (3), 31−40.

(11) Kanak, S.; Verma, A. Evaluation of antimicrobial and anticancer activities of methanol extract of in vivo and in vitro grown *Bauhinia variegata* L. *Int. Res. J. Biol. Sci.* **2012**, *1* (6), 26−30.

(12) Hegde Chaitra, R.; et al. Evaluation of antimicrobial properties, phytochemical contents and antioxidant capacities of leaf extracts of *Punica granatum* L. *ISCA J. Biol. Sci.* **2012**, *1* (2), 32−37.

(13) Philippe, S.; et al. In vitro Antifungal activities of Essential oils extracted from Fresh Leaves of Cinnamomum zeylanicum and Ocimum gratissimum against Foodborne pathogens for their use as Traditional Cheese Wagashi conservatives. *Res. J. Recent Sci.* **2012**, *1* (9), 67−73.

(14) Sribhurathy, V.; Rejendran, S. Corrosion inhibition by green inhibitor: sodium metavanadate-spirulina system. *Chem. Sci. Rev. Lett.* **2012**, *1* (1), 25−29.

(15) Fouda, A.; et al. CalicotomeExtract as a friendly corrosion inhibitor forCarbon steel in polluted NaClSolution: chemical and electrochemical studies. *Egypt. J. Chem.* **2019**, *62* (10), 1879−1894.

(16) Antony, N.; Sherine, H. B.; Rajendran, S. Inhibition and biocide actions of sodium dodecyl sulfate-Zn2+ system for the corrosion of carbon steel in chloride solution. *Port. Electrochim. Acta* **2010**, *28* (1), 1−14.

(17) Wang, Y.; Qiang, Y.; Zhi, H.; et al. Evaluating the synergistic effect of maple leaves extract and iodide ions on corrosion inhibition of Q235 steel in H2SO4 solution. *J. Ind. Eng. Chem.* **2023**, *117*, 422−433, DOI: 10.1016/j.jiec.2022.10.030.

(18) Wang, Q.; Zhao, C.; Zhang, Q.; et al. Synergistic Effect of Benincasa hispida Peel Extract and KI on the Corrosion Inhibition of Mild Steel in HCl. *Sustainability* **2023**, *15* (14), 11370.

(19) Al Jahdaly, B. A. Rosmarinus officinalis extract as eco-friendly corrosion inhibitor for copper in 1 M nitric acid solution: Experimental and theoretical studies. *Arabian J. Chem.* **2023**, *16* (1), No. 104411.

(20) Begum, A. A.; Vahith, R. M.; Mohamed, M. K.; et al. Corrosion mitigation on orthodontic wire made of SS 18/8 alloy using esomeprazole tablet (Esiloc-40 mg) in artificial saliva. *J. Saudi Chem. Soc.* **2023**, *27* (4), No. 101681, DOI: 10.1016/j.jscs.2023.101681.

(21) Dewangan, Y.; Verma, D. K.; Berdimurodov, E.; et al. N-hydroxypyrazine-2-carboxamide as a new and green corrosion inhibitor for mild steel in acidic medium: experimental, surface morphological and theoretical approach. *J. Adhes. Sci. Technol.* **2022**, *36* (23−24), 2644−2664.

(22) Berdimurodov, E.et al. Chapter 23 - Pharmaceutical Drugs as Prominent Corrosion Inhibitors: Fundamental and Computational Aspects of Density Functional Theory. In *Computational Modelling and Simulations for Designing of Corrosion Inhibitors*; Elsevier, 2023; pp 461−479 DOI: 10.1016/B978-0-323-95161-6.00005-9.

(23) Berdimurodov, E.; Kholikov, A.; Akbarov, K.et al.Grafted Chitosan as Sustainable Corrosion Inhibitors. In *Grafted Biopolymers as Corrosion Inhibitors: Safety, Sustainability, and Efficiency* 2023; pp 285−312 DOI: 10.1002/9781119881391.ch13.

(24) Berdimurodov, E.; Kholikov, A.; Akbarov, K.; et al. A gossypol derivative as an efficient corrosion inhibitor for St2 steel in 1 M HCl+ 1 M KCl: An experimental and theoretical investigation. *J. Mol. Liq.* **2021**, *328*, 115475.

(25) Shahmoradi, A.; Ranjbarghanei, M.; Javidparvar, A.; et al. Theoretical and surface/electrochemical investigations of walnut fruit green husk extract as effective inhibitor for mild-steel corrosion in 1M HCl electrolyte. *J. Mol. Liq.* **2021**, *338*, 116550 DOI: 10.1016/j.molliq.2021.116550.

(26) Etaiw, S. E. H.; Hassan, G. S.; El-Hossiany, A. A.; et al. Nano-metal−organic frameworks as corrosion inhibitors for strengthening anti-corrosion behavior of carbon steel in a sulfuric acid environment: from synthesis to applications. *RSC Adv.* **2023**, *13* (22), 15222−15235.

(27) Fouda, A. S.; Abdel-Wahed, H. M.; Atia, M. F.; et al. Novel porphyrin derivatives as corrosion inhibitors for stainless steel 304 in acidic environment: synthesis, electrochemical and quantum calculation studies. *Sci. Rep.* **2023**, *13* (1), No. 17593.

(28) Hashmi, A. W.; Mali, H. S.; Meena, A.; et al. Surface characteristics improvement methods for metal additively manufactured parts: A review. *Adv. Mater. Process. Technol.* **2022**, *8* (4), 4524−4563.

(29) Keshtov, M. L.; Konstantinov, I. O.; Khokhlov, A. R.; et al. New wide band gap π-conjugated copolymers based on anthra [1, 2-b: 4, 3-b′: 6, 7-c″] trithiophene-8, 12-dione for high performance non-fullerene polymer solar cells with an efficiency of 15.07%. *Polymer* **2022**, *251*, 124892.

(30) Khaled, M. A.; Ismail, M. A.; El-Hossiany, A. A.; et al. Novel pyrimidine-bichalcophene derivatives as corrosion inhibitors for copper in 1 M nitric acid solution. *RSC Adv.* **2021**, *11* (41), 25314−25333.

(31) Salem, A.; Wahba, A.; Hossiany, A. E.; et al. Experimental and computational chemical studies on the corrosion inhibitive properties

of metamizole sodium pharmaceutical drug compound for CS in hydrochloric acid solutions. *J. Indian Chem. Soc.* **2022**, *99* (12), No. 100778.
(32) Tan, B.; He, J.; Zhang, S.; et al. Insight into anti-corrosion nature of Betel leaves water extracts as the novel and eco-friendly inhibitors. *J. Colloid Interface Sci.* **2021**, *585*, 287−301.
(33) Ahmad, K.; Asif, H. M.; Afzal, T.; et al. Green synthesis and characterization of silver nanoparticles through the Piper cubeba ethanolic extract and their enzyme inhibitory activities. *Front. Chem.* **2023**, *11*, 1065986.
(34) Dwita, L. P.; et al. BRAIN ANTIOXIDANT PROPERTIES OF PIPER CUBEBA L. EXTRACTS AND ESSENTIAL OIL. *Farmacia* **2023**, *71* (2), 296−302.
(35) Kadhim, M. M.; Khadom, A. A.; Mahdi Rheima, A.; et al. On the influence of hydrocarbons solvents on the inhibition efficiency of some organic corrosion inhibitors: Theoretical and validation studies. *J. Mol. Liq.* **2023**, *377*, 121538.
(36) Xiao, J.; Long, X.; Qu, W.; et al. Influence of sulfuric acid corrosion on concrete stress−strain relationship under uniaxial compression. *Measurement* **2022**, *187*, 110318.
(37) Kadhim, A.; et al. Corrosion inhibitors. A review. *Int. J. Corros. Scale Inhib.* **2021**, *10* (1), 54−67.
(38) Drissi, B.; Mahdi, I.; Yassir, M.; et al. Cubeb (*Piper cubeba* Lf): A comprehensive review of its botany, phytochemistry, traditional uses, and pharmacological properties. *Front. Nutr.* **2022**, *9*, 1048520.
(39) Gusson-Zanetoni, J. P.; da Silva, J. S. G. M.; Picão, T. B.; et al. Effect of Piper cubeba total extract and isolated lignans on head and neck cancer cell lines and normal fibroblasts. *J. Pharmacol. Sci.* **2022**, *148* (1), 93−102.
(40) Zheng, H. f.; Yu, S.; Hu, T. d.; et al. CAl 3 X (X = B/Al/Ga/In/Tl) with 16 valence electrons: can planar tetracoordinate carbon be stable? *Phys. Chem. Chem. Phys.* **2018**, *20* (41), 26266−26272.
(41) Becke, A. D. Density-functional thermochemistry. I. The effect of the exchange-only gradient correction. *J. Chem. Phys.* **1992**, *96* (3), 2155−2160.
(42) Stephens, P. J.; Devlin, F. J.; Chabalowski, C. F.; et al. Ab initio calculation of vibrational absorption and circular dichroism spectra using density functional force fields. *J. Phys. Chem. A* **1994**, *98* (45), 11623−11627.
(43) Barone, V.; Cossi, M. Quantum calculation of molecular energies and energy gradients in solution by a conductor solvent model. *J. Phys. Chem. A* **1998**, *102* (11), 1995−2001.
(44) Delley, B. An all-electron numerical method for solving the local density functional for polyatomic molecules. *J. Chem. Phys.* **1990**, *92* (1), 508−517.
(45) Delley, B. From molecules to solids with the DMol 3 approach. *J. Chem. Phys.* **2000**, *113* (18), 7756−7764.
(46) Becke, A. D. A multicenter numerical integration scheme for polyatomic molecules. *J. Chem. Phys.* **1988**, *88* (4), 2547−2553, DOI: 10.1063/1.454033.
(47) Boese, A. D.; Handy, N. C. A new parametrization of exchange−correlation generalized gradient approximation functionals. *J. Chem. Phys.* **2001**, *114* (13), 5497−5503.
(48) Reed, A. E.; Weinstock, R. B.; Weinhold, F. Natural population analysis. *J. Chem. Phys.* **1985**, *83* (2), 735−746, DOI: 10.1063/1.449486.
(49) Ansari, K.; Quraishi, M. Experimental and quantum chemical evaluation of Schiff bases of isatin as a new and green corrosion inhibitors for mild steel in 20% H2SO4. *J. Taiwan Inst. Chem. Eng.* **2015**, *54*, 145−154.
(50) Saleh, T. A.; Haruna, K.; Nur, M. M.; et al. Synthesis of Amine Grafted Poly (Acrylic-Maleic) as an efficient inhibitor against stainless steel corrosion in a highly saline medium. *Prog. Org. Coat.* **2022**, *170*, 106974.
(51) Sherine, B.; Nasser, A. A.; Rajendran, S. Inhibitive action of hydroquinone-Zn2+ system in controlling the corrosion of carbon steel in well water. *Int. J. Eng. Sci. Technol.* **2010**, *2* (4), 341−357.
(52) Fouda, A. E. A. S.; Etaiw, S. E. H.; Sobhy, S. Metal-organic frameworks based on heterocyclic ligands and some transition metals as effective carbon steel corrosion inhibitors in aqueous environment. *J. Mol. Liq.* **2022**, *348*, 118402 DOI: 10.1016/j.molliq.2021.118402.
(53) Abdel−Rahim, S. S.; Khaled, K. F.; Abd−Elshafi, N. S. Electrochemical frequency modulation as a new technique for monitoring corrosion inhibition of iron in acid media by new thioureas derivative. *Electrochim. Acta* **2006**, *51* (16), 3269−3377, DOI: 10.1016/j.electacta.2005.09.018.
(54) Ismail, M. A.; Shaban, M. M.; Abdel-Latif, E.; et al. Novel cationic aryl bithiophene/terthiophene derivatives as corrosion inhibitors by chemical, electrochemical and surface investigations. *Sci. Rep.* **2022**, *12* (1), No. 3192.
(55) Bouklah, M.; Hammouti, B.; Lagrenée, M.; et al. Thermodynamic properties of 2, 5-bis (4-methoxyphenyl)-1, 3, 4-oxadiazole as a corrosion inhibitor for mild steel in normal sulfuric acid medium. *Corros. Sci.* **2006**, *48* (9), 2831−2842.
(56) Li, X.; Deng, S.; Fu, H. Adsorption and inhibition effect of vanillin on cold rolled steel in 3.0 M H3PO4. *Prog. Org. Coat.* **2010**, *67* (4), 420−426.
(57) Ferreira, E.; Giacomelli, C.; Giacomelli, F.; et al. Evaluation of the inhibitor effect of L-ascorbic acid on the corrosion of mild steel. *Mater. Chem. Phys.* **2004**, *83* (1), 129−134.
(58) Liu, G.; Xue, M.; Yang, H. Polyether copolymer as an environmentally friendly scale and corrosion inhibitor in seawater. *Desalination* **2017**, *419*, 133−140.
(59) Yadav, M.; Sharma, U.; Yadav, P. RETRACTED ARTICLE: Corrosion inhibitive properties of some new isatin derivatives on corrosion of N80 steel in 15% HCl. *Int. J. Ind. Chem.* **2013**, *4*, 1−10.
(60) Sudheer; Quraishi, M. Thermodynamic and Electrochemical Investigation of Pantoprazole:{(RS)-6-(difluoromethoxy)-2-[(3, 4-dimethoxypyridin-2-yl) methylsulfinyl]-1 H-benzo [d]-imidazole} as Corrosion Inhibitor for Mild Steel in Hydrochloric Acid Solution. *Arabian J. Sci. Eng.* **2013**, *38* (1), 99−109.
(61) Elgyar, O. A.; et al. The inhibition action of viscum album extract on the corrosion of carbon steel in hydrochloric acid solution. *Biointerface Res. Appl. Chem.* **2021**, *11* (6), 14344−14358.
(62) Fouda, A. S.; Ahmed, R.; El-Hossiany, A. Chemical, electrochemical and quantum chemical studies for famotidine drug as a safe corrosion inhibitor for α-brass in HCl solution. *Prot. Met. Phys. Chem. Surf.* **2021**, *57* (2), 398−411.
(63) Lenderink, H.; Linden, M.; De Wit, J. Corrosion of aluminium in acidic and neutral solutions. *Electrochim. Acta* **1993**, *38* (14), 1989−1992.
(64) El Hamdani, N.; Fdil, R.; Tourabi, M.; et al. Alkaloids extract of *Retama monosperma* (L.) Boiss. seeds used as novel eco-friendly inhibitor for carbon steel corrosion in 1 M HCl solution: Electrochemical and surface studies. *Appl. Surf. Sci.* **2015**, *357*, 1294−1305.
(65) Sherif, E.; Park, S. M. Effects of 1, 4-naphthoquinone on aluminum corrosion in 0.50 M sodium chloride solutions. *Electrochim. Acta* **2006**, *51* (7), 1313−1321.
(66) Fouda, A. S.; Abdel-Latif, E.; Helal, H. M.; et al. Synthesis and characterization of some novel thiazole derivatives and their applications as corrosion inhibitors for zinc in 1 M hydrochloric acid solution. *Russ. J. Electrochem.* **2021**, *57*, 159−171.
(67) Muthukrishnan, P.; Jeyaprabha, B.; Prakash, P. Mild steel corrosion inhibition by aqueous extract of *Hyptis Suaveolens* leaves. *Int. J. Ind. Chem.* **2014**, *5*, 1−11.
(68) Fouda, A.; Azeem, M. A.; Mohamed, S.; et al. Corrosion inhibition and adsorption behavior of nerium oleander extract on carbon steel in hydrochloric acid solution. *Int. J. Electrochem. Sci.* **2019**, *14* (4), 3932−3948.
(69) Kosari, A.; Moayed, M.; Davoodi, A.; et al. Electrochemical and quantum chemical assessment of two organic compounds from pyridine derivatives as corrosion inhibitors for mild steel in HCl solution under stagnant condition and hydrodynamic flow. *Corros. Sci.* **2014**, *78*, 138−150.
(70) Haldhar, R.; Prasad, D.; Bhardwaj, N. Extraction and experimental studies of Citrus aurantifolia as an economical and green corrosion inhibitor for mild steel in acidic media. *J. Adhes. Sci. Technol.* **2019**, *33* (11), 1169−1183.

https://doi.org/10.1021/acsomega.3c09334
ACS Omega 2024, 9, 5024−5037

(71) Elabbasy, H. M.; Fouda, A. Olive leaf as green corrosion inhibitor for C-steel in Sulfamic acid solution. *Green Chem. Lett. Rev.* **2019**, *12* (3), 332−342.
(72) Ali, A. E.; Badr, G. E.; Fouda, A. Citrus sinensis extract as a green inhibitor for the corrosion of carbon steel in sulphuric acid solution. *Biointerface Res. Appl. Chem.* **2021**, *11*, 14007−14020.
(73) Fouda, A. S.; Ibrahim, A. Aqueous extract of juniperus as a green corrosion inhibitor for mild steel (MS) in Sulfamic acid (NH 2 SO 3 H) solutions. *Prot. Met. Phys. Chem. Surf.* **2018**, *54*, 1194−1203.
(74) Chung, I. M.; Kim, S. H.; Hemapriya, V.; et al. Inhibition behavior of *Tragia involucrata* L. phenolic compounds against acidic medium corrosion in low carbon steel surface. *Chin. J. Chem. Eng.* **2019**, *27* (3), 717−725.
(75) Fouda, A.; et al. Corrosion inhibition and thermodynamic activation parameters of *Myrtus communis* extract on mild steel in sulfamic acid medium. *Int. J. Corros. Scale Inhib.* **2017**, *6* (4), 428−448.

https://doi.org/10.1021/acsomega.3c09334
ACS Omega 2024, 9, 5024−5037